Research Article | Vol. 33, No. 10 / 19 May 2025 / Optics Express 20656
Optics EXPRESS

Arbitrary pulse shaping in a mid-infrared optical parametric oscillator source

EDCEL J. SALUMBIDES,[1] YOUSSEF EZZO,[1] ZEUDI MAZZOTTA,[1] WIM UBACHS,[1,2] KJELD S. E. EIKEMA,[1,2] OSCAR VERSOLATO,[1,2,4] AND STEFAN WITTE[1,2,3,*]

[1]*Advanced Research Center for Nanolithography (ARCNL), Science Park 106, 1098 XG Amsterdam, The Netherlands*
[2]*Department of Physics and Astronomy and LaserLab, Vrije Universiteit Amsterdam, De Boelelaan 1081, 1081 HV Amsterdam, The Netherlands*
[3]*Present address: Imaging Physics Department, Faculty of Applied Sciences, Delft University of Technology, Lorentzweg 1, 2628 CJ Delft, The Netherlands*
[4]*o.versolato@arcnl.nl*
[*]*s.witte@arcnl.nl*

Abstract: We present a coherent mid-infrared (mid-IR) light source based on a periodically poled lithium niobate optical parametric oscillator (OPO) that is capable of producing arbitrary pulse shapes in the nanosecond regime. By controlling the shape of the 1064-nm wavelength pump, we compensate for the cavity dynamics that enable temporal pulse shaping of the mid-IR output for a signal wavelength of 1.9 μm (with a corresponding idler wavelength of 2.4 μm). Examples of complex pulse profiles demonstrate the versatility in temporal shaping of the OPO output. This low-energy mid-IR source, delivering pulses of around 1 mJ, is ideally suited to provide temporally optimized seed radiation for further high-energy amplification.

Published by Optica Publishing Group under the terms of the Creative Commons Attribution 4.0 License. Further distribution of this work must maintain attribution to the author(s) and the published article's title, journal citation, and DOI.

1. Introduction

Tunable mid-infrared (mid-IR) radiation sources that can offer broad wavelength coverage, narrow spectral bandwidth, and high power or energy are needed in many applications [1–3] including spectroscopy, high-harmonic generation, imaging, biomedical diagnosis, material, and industrial processing, as well as distance ranging and military counter-defenses. An important class of mid-IR sources is based on optical parametric oscillators (OPO) and optical parametric amplifiers (OPA). These optical sources based on nonlinear frequency conversion extend access to wavelength ranges where no tunable laser systems exist, for example in the mid-IR region. With continuous advances in the fabrication of nonlinear materials, efficient optical conversion and high-energy output can be achieved [4–7]. Attractive features of OPO's include a simple cavity design, broad wavelength tunability, and a wide range in temporal profiles spanning from cw through to femtosecond pulse widths [8–10]. Radiation sources emitting high-energy nanosecond pulses at 2–10 μm wavelengths are of particular relevance to the generation of extreme ultraviolet (EUV) light for EUV lithography [11]. Such driving pulses of several hundred mJ are imaged onto sub-mm tin targets to create EUV-emitting plasma. Central to the achievement of the highest conversion efficiencies of the drive laser pulse energy into useful EUV radiation is the full geometrical overlap of the laser profile and the tin target [12], as well as a top-hat temporal pulse shape [13]. In such applications, the OPO output is used as seed radiation for a subsequent optical parametric amplification (OPA) stage. However, the complex OPO cavity build-up dynamics strongly influences the output pulse shape. These dynamics can be a limiting factor in obtaining

#559462 https://doi.org/10.1364/OE.559462
Journal © 2025 Received 19 Feb 2025; revised 28 Mar 2025; accepted 2 Apr 2025; published 7 May 2025

Optics EXPRESS

the maximum amplification efficiency in the OPA if this results in a suboptimal temporal overlap of the OPO seed output and OPA pump.

In this paper, we describe an OPO operation in which the temporal cavity dynamics is controlled by tailoring the temporal shape of the pump laser. This allows controlling the build-up time to be as short as possible, resulting in the output of the OPO signal having a square temporal profile that is required in our experiments on plasma EUV generation [13]. This capability is made possible with the use of an advanced 1064-nm pump laser source, which can deliver temporally programmable pulse shapes, developed in our laboratory [14]. As the nonlinear medium of the OPO, we make use of a 10-channel periodically-poled lithium niobate (PPLN) device, with channels chosen to have different poling periods, which together with temperature tuning allows broadband wavelength tunability from 1.4 to 4.4 μm [15,16]. The high level of temporal control of the pump input could be exploited to produce an OPO output in the mid-infrared with arbitrary temporal profiles that may be useful in other advanced applications, such as in laser ignition facilities [17,18].

2. Experiment

A schematic representation of the setup is shown in Fig. 1. The pump laser system used, which delivers 1064-nm pulses with excellent temporal shaping capability, was developed at our institute and has been described previously by Meijer et al. [14]. While this pump laser can deliver up to hundreds of mJ (also depending on the pulsewidth), only a small portion is split off to provide up to 10 mJ, which is sufficient for pumping the OPO. The OPO requires a collimated Gaussian pump beam of ~800 μm $1/e^2$-diameter, which is obtained by placing a demagnifying telescope in the pump beam. A 400 μm diameter circular aperture is placed at the focus for spatial filtering purposes. A 50 mm long periodically poled lithium niobate (PPLN) device (HC Photonics Corp.), housed in a temperature-controlled oven, is used as the nonlinear material. This PPLN device contains ten channels with different poling periods ranging from 27.6 to 31.6 μm, which enable the tuning of wavelengths between 1.4 and 4.5 μm (collective range for both signal and idler). Two flat mirrors define the optical cavity, with a high-reflectivity input coupler (99.8% reflectivity for 1.4 – 2.1 μm) and an output coupler with around 14% transmission for the signal wavelength at 1.9 μm. Both cavity mirrors are antireflection coated for the 1064-nm wavelength pump beam. Here, we demonstrate the operation of OPO for a signal wavelength of 1.9 μm (with a corresponding idler wavelength of 2.4 μm), using the PPLN channel with the longest poling period and with the oven temperature set at 190° C. We have performed preliminary tests of OPO operation at other signal wavelengths, including temporal shaping, and found similar behavior as described here for 1.9 μm. The polarizations of the pump input, signal, and idler outputs are linear and are all aligned along the vertical. The OPO

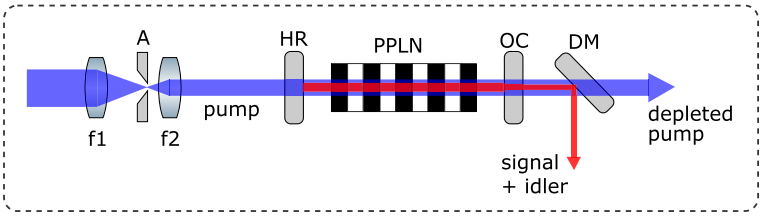

Fig. 1. A schematic diagram of the OPO setup is shown; f1, f2: lenses; A: spatial filter; HR: high-reflector for signal wave (high-transmitter for pump); OC: output coupler; PPLN: nonlinear material; DM: dichroic mirror. The OPO signal output is steered towards diagnostic instruments. The depleted pump is also monitored.

Optics EXPRESS

signal energy conversion efficiency is about 18–23%, delivering a signal output of up to 1 mJ with a good spatial beam profile and an estimated M^2 value of <1.5. After the OPO cavity, a dichroic mirror is used to reflect the signal wavelength, with the transmitted pump monitored for depletion. Transmission spectral filters are used downstream in the signal beam path for further spectral separation. Separate fast photodiodes (EOT ET5000), connected to a 4-GHz bandwidth oscilloscope (Keysight DSO9404A), are used to monitor pump and signal temporal profiles. The electronic time delay between the photodiodes and cable connections was measured and compensated for in the temporal analysis described below.

3. Results and discussions

In this study we present results at $\lambda = 1.9$ μm, which is representative of the behavior for other wavelengths in our OPO tuning range. The OPO signal output exhibits a temporal profile reminiscent of a logistic growth curve when pumped with a top-hat (or square) pulse, as shown in Fig. 2(a). The periodic oscillation in the temporal profiles of Fig. 2(a) corresponds to the round-trip period of the signal cavity of $\tau_{cav} = 1.09$ ns, resulting from the interference of multiple modes circulating in the cavity. This measured round-trip period is consistent with the cavity length expected for the resonator distances and the crystal length. We first compare the signal output obtained from a top-hat pump with an energy amplitude of 2.3 mJ and pulsewidth of 20 ns (pump intensity $I_p = 29.6$ MW/cm^2) shown as the blue curve in Fig. 2(a), and the OPO output from a top-hat pump with an energy of 0.90 mJ and pulsewidth of 20 ns ($I_p = 11.7$ MW/cm^2) shown as the green curve in the same figure. The buildup is faster at higher pump energy, leading to earlier signal emission compared to a lower pump energy. As expected, the higher-energy

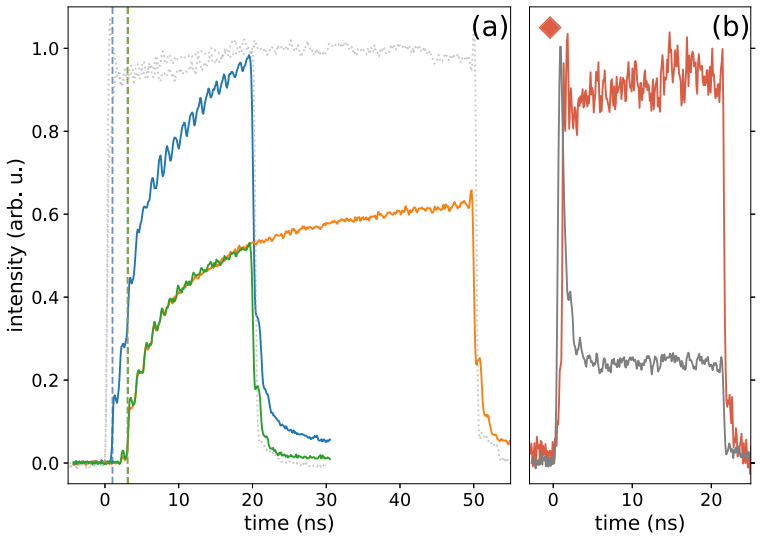

Fig. 2. Temporal profiles of the OPO signal output. (a) The green, orange, and blue curves are produced by a top-hat pump profile with intensities of 12 MW/cm^2 (20 ns), 12 MW/cm^2 (50 ns), 30 MW/cm^2 (20 ns), respectively. The 20-ns and 50-ns pump profiles are plotted as gray dotted curves. The OPO outputs in (a) share the same relative intensity scaling. The vertical dashed lines indicate the measured build-up time τ_{bu} of the OPO outputs with respect to the pump which is used to set $t = 0$. (b) For comparison, a signal output with top-hat temporal profile (red curve) is also shown, obtained using a non-top hat but an optimally shaped pump profile (gray curve), see the main text. The red data marker serves as reference for Fig. 3.

Optics EXPRESS

(blue) curve also reaches a higher final amplitude compared to the lower-energy (green) curve at the end of the pump pulse at 20 ns. This behavior is expected, given the non-linear nature of the parametric process that depends on the threshold intensity I_{th} and the pump intensity I_p. This is further demonstrated by another comparison with the OPO output of a top-hat pump with an energy of 2.3 mJ and a longer pulse width of 50 ns (I_p = 11.7 MW/cm^2) shown as the orange profile in Fig. 2(a). The green and orange traces, having the same pump intensity but with different pump pulse widths of, respectively, 20 and 50 ns, show perfect overlap in their time evolution. The use of different pump temporal shapes leads to different temporal OPO output profiles; an example is shown in Fig. 2(b), where the top-hat signal profile (in red) is obtained with a tailored pump profile (in gray), as discussed in more detail below.

Before demonstrating the control and optimization of the cavity dynamics, we first turn to quantifying the cavity response to a temporally top-hat profile. We define a cavity build-up time parameter τ_{bu} as the elapsed time for the signal output to reach 10% of its maximum intensity, as graphically represented in Fig. 2(a). This time interval is measured relative to the $t = 0$ position taken as the on-time of top-hat pump intensity (when it reaches its half-maximum). Note that our definition for τ_{bu} differs from those used in the literature from the perspective of theoretical or analytical studies [19,20], which relate the build-up of a minimum detectable signal with respect to the absolute quantum noise floor. This approach is not easily implemented in the experiment, and instead we opt for our more robust, empirical 10%-threshold definition. Note that the exact value of this threshold does not affect the temporal pulse shape optimization procedure discussed below, and only leads to a scale factor on τ_{bu}. Our present definition then enables us to compare the results between two experiments, where one is our current PPLN-based OPO setup and the other is a KTP-based OPO setup [13], with measurements made under otherwise identical conditions in the same laboratory. There may be limitations in a quantitative comparison of τ_{bu}, especially when comparing signal output shapes with qualitatively different signal profiles. For this reason, we limit our direct comparison of τ_{bu} for the case of top-hat pump input pulses, where we only vary the pump energy (and hence intensity I_p) while keeping the pump pulse width constant at 20 ns.

The extracted OPO signal build-up times τ_{bu} are plotted in Fig. 3 (left panel) as the top-hat pump input intensity is varied. The build-up time shows a trend towards shorter τ_{bu} values with higher pump energies. The indicated error bars are dominated by systematic errors due to the cavity oscillations and slow logistic build-up function for long build-up times, while the oscilloscope sampling speed limits that for the short build-up times. Representative temporal profiles for the PPLN OPO operation leading to build-up times of 3.0, 1.0 and 0.8 ns are plotted in the right panels of Fig. 3. These temporal traces exhibit a change in shape towards a steeper increase and amplitude saturation accompanying shorter build-up times. As seen in the left panel of Fig. 3, the PPLN OPO leads to much shorter build-up times compared to the KTP OPO in Ref. [13], from which the KTP τ_{bu} dataset is reproduced here. The shorter build-up time for the case of PPLN relative to KTP is expected when comparing the non-linear intensity thresholds for these materials. For the 5-cm PPLN crystal length in this study, we obtained a characteristic irradiance of $I_{th,calc}$ = 0.25 MW/cm^2 calculated from the definition given in Eq. (1.25) of Ref. [21], for the present signal and idler wavelengths. In contrast, the characteristic irradiance for the 1.8 cm long KTP crystal used in Ref. [13] is much higher at $I_{th,calc}$ = 38 MW/cm^2, leading to a higher pump intensity requirement to induce parametric oscillation for KTP.

Inspired by Refs. [13,19], we express the cavity build-up time τ_{bu} as:

$$\tau_{bu} = \frac{\tau_{cav}}{A\sqrt{I_p/I_{th,calc}} - B}, \tag{1}$$

where τ_{cav} is the resonator roundtrip time of the signal wavelength and I_p is the input pump intensity. Despite the shorter KTP OPO cavity with a round-trip time of $\tau_{cav,KTP}$ = 0.30 ns [13]

Optics EXPRESS

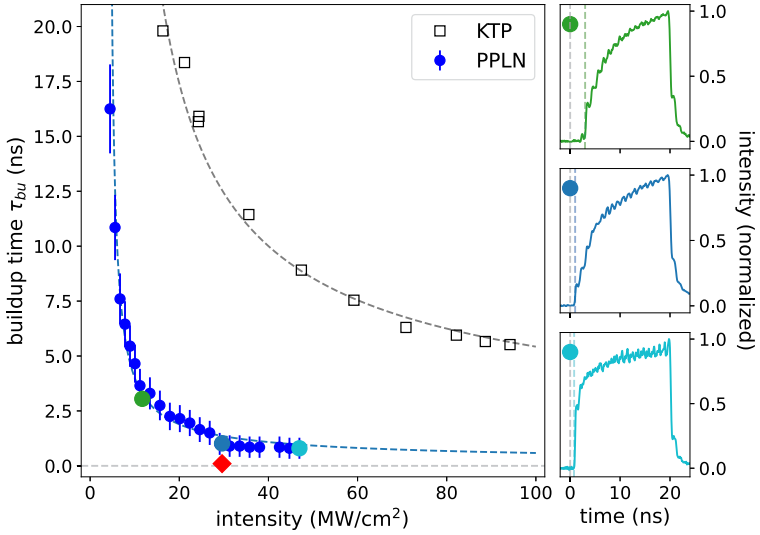

Fig. 3. (Left) Build-up times τ_{bu} of the PPLN OPO signal output (blue circles) as a function of the intensity I_p of a top-hat pump. For comparison, the build-up times of a KTP OPO, described previously by Behnke et al. [13], are plotted (unfilled squares). Line fits using Eq. (1) are also plotted for each build-up time dataset. (Right) Temporal profiles corresponding to three representative build-up time datapoints are shown. Dashed vertical lines indicate the onset of the pump (at t=0, gray) and when the 10% threshold intensity is obtained, defining the build-up time. The top and middle panels are the same curves as shown in Fig. 2(a), with a 20-ns top-hat pump pulse. The datapoint in red (diamond) in the left panel indicates the build-up time of the optimized top-hat signal output shown in Fig. 2(b) [see text].

compared to $\tau_{cav,PPLN}$ = 1.1 ns, the PPLN OPO exhibits much shorter build-up times as seen in Fig. 3. The optimal fits based on Eq. (1) for both the PPLN and KTP datasets are also plotted in Fig. 3, demonstrating that the simple relation adopted here adequately describes the behavior of cavity build-up time. Equation (1) is a simplified form related to the analytical expression derived by Godard et al. [20], which however does not include optical losses from, for example, absorption or scattering. Eq. (1) is also consistent with the relation used previously in Ref. [13] for the analysis of a KTP-based OPO, with an appropriate redefinition of the parameters. In the analysis in Ref. [13], three parameters were fitted, including the characteristic threshold energy E_{th}, which corresponds to I_{th} here, but that leads to an overdetermined fit that couples the fit parameters. In the present analysis, we fix $I_{th,calc}$ to the calculated values [22] and only fit the parameters A and B. The parameters extracted from the PPLN fitting procedure are A_{PPLN} = 0.082 and B_{PPLN} = 0.29, while the KTP analysis yields A_{KTP} = 0.040 and B_{KTP} = 0.013. One can interpret the A parameter as describing an effective feedback factor that promotes signal gain, and the B parameter as accounting for the effective losses. Remarkably, such counterbalancing influences that depend on mirror reflectivities, absorption, scattering, and alignment losses leading to complex nonlinear oscillator dynamics in different setups are nevertheless shown to be well captured by the approximate relation in Eq. (1). Although the A parameters for both the PPLN and KTP cases are comparable (within a factor of 2), the B parameters are different by a factor of 20, leading to an interpretation of much higher losses of the signal wave for the PPLN OPO relative to the KTP OPO. If the B parameters had been comparable, we would expect an even much faster build-up for the PPLN OPO by a factor $\sqrt{I_{th,KTP}/I_{th,PPLN}} \sim 12$.

Optics EXPRESS

We can use the obtained understanding of the cavity dynamics to optimize its response. Specifically, we demonstrated that build-up times below 1 ns are feasible at modest intensities of several 10 MW/cm^2 using long, 20-ns flattop pulses. The build-up time may be expected to reduce further with higher intensity. To compensate for the slow intensity rise in the beginning of the signal build-up in the case of a top-hat pump input, one can choose a pump input profile with a much higher intensity amplitude at the very beginning of the pulse to prompt the initial signal build-up. To mitigate any fluence damage thresholds, the intensity should be sustained for a minimum duration, and we opt for reducing the pump to a lower, constant intensity after this initial high-intensity burst. We demonstrate this approach with good results, with the special example shown in Fig. 2(b) of a top-hat OPO signal output. The tailored pump temporal profile was obtained by active optimization of the pump shape shown as the gray curve in Fig. 2(b). The build-up time of 0.1 ns for this top-hat OPO signal output is plotted in Fig. 3 as the red (diamond) datapoint (taking an *averaged* intensity of 30 MW/cm^2 over the 20-ns pump pulse duration), also corresponding to Fig. 2(b). Considering that the instantaneous intensity burst is only 150 MW/cm^2, the measured τ_{bu} = 0.1 ns is much shorter than would be expected for the PPLN fit function in Fig. 3 (i.e., this is much shorter than the extrapolated τ_{bu} value from the fit function for that peak intensity). Note also that the 0.1 ns build-up time in this example is much shorter than the cavity round-trip time and could be interpreted as transient optical parametric generation before the onset of the cavity feedback.

The capability to manipulate the signal output's temporal profile can be extended towards tailoring much more complex outputs, with examples shown in Fig. 4(a) and (b). For these complex temporal shapes, an initial EOM profile is provided that is iterated in a completely autonomous and automated optimization procedure. For the first example, the output temporal profile (blue) and the target profile (gray) are both shown in the upper panel (a) comprising several ramp-up and ramp-down events that resemble pyramidical (or triangular) structures. The corresponding pump input profile (orange) is shown in the bottom panel (c), along with the depleted pump temporal profile (green). To obtain these output pulses, an initial high-intensity pump input is needed to prime the OPO dynamics, where the signal wave takes some time to build up. This initial pump intensity burst needs to be turned down abruptly to ensure that the resulting output follows linear growth. Otherwise, if the pump intensity is maintained for longer, a logistic growth in the signal output would evolve instead (for example, those depicted in Fig. 2(a)). The effect of this initial pump pulse burst is not converted into a top-hat feature in the signal output. This is consistent when looking at the pump depletion, which shows hardly any difference with the pump input for the leading burst feature. This tiny amount of parametric signal generation serves as a seeding primer that is essential to produce the linear ramp in the first triangular output structure. The nonlinear gain effect in the parametric process can be seen by comparing the peak heights of the first two pyramidal structures of the OPO output. Notice that the peak height difference of the first two structures is more pronounced in the signal output than in the input pump pulse shape. Such advanced output profiles may be useful for applications where fast (nanoseconds) ramping (up- or down-) events are required.

Another example of a nontrivial signal output pulse profile is shown in Fig. 4(b). The target profile (gray dashed curve) and the resulting signal output profile (blue curve) are demonstrations of a complex train of box pulses with arbitrary amplitudes, pulse widths, and gaps between the pulse features. In the lower panel of Fig. 4(d), the corresponding pump profile input is shown as the orange trace, while the depleted pump is also shown as the green trace. The depleted pump, indicating the unconverted pump energy, sheds some light on the parametric conversion process. Although there is some correlation in the input and output profiles, the non-linearity in the OPO cavity dynamics is apparent particularly at early times. We note that the difference in the onset behavior is mainly determined by the intensity of the pump, which was somewhat higher in panel (d) than in panel (c). After the onset of conversion, the signal closely but non-linearly follows the

Optics EXPRESS

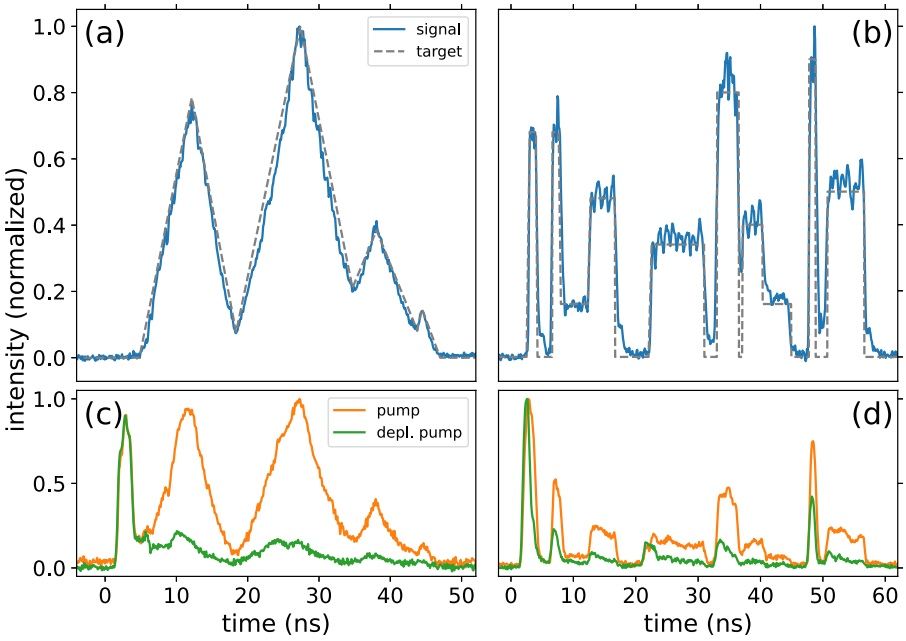

Fig. 4. Examples of arbitrary temporal shaping of the OPO signal output (individually normalized). (a) A series of ramp-up and ramp-down events resemble pyramidical structures. The experimental data is shown in blue and the target temporal profile in gray. (b) A complex train of mid-IR top-hat pulses, with various amplitudes widths and time gaps, resembling a city skyline. The input pump profile (orange) and the depleted pump profile (green) are shown in the lower panels, where (c) corresponds to (a), and (d) corresponds to (b), respectively.

pump. These subtle yet impactful details highlight the good level of temporal shaping control required. Such a complex train of pulses can be of interest as seeding radiation for high-energy laser systems that are used in investigations at advanced laser ignition facilities [17,23].

4. Conclusions

We have shown tailored temporal shaping of the mid-IR output of an optical parametric oscillator, demonstrated here for 1900-nm wavelengths with sub-mJ output energies, by controlling the temporal shape of the 1064-nm wavelength pump input. An analysis of the build-up times provides insight into the cavity dynamics of the PPLN-based OPO in this study, which can be compared to that of a different KTP-based OPO. The build-up times are captured well by a semiempirical formula, which explains the much shorter build-up times obtained for the current PPLN-based OPO. By exploiting the temporal dynamics of the signal (and idler) wave building up in the cavity, arbitrary temporal shaping capability of the output is demonstrated from flat-top profiles to more complex pulse trains. The quality of such top-hat profiles is of particular importance in the optimization of light conversion efficiency in plasma-driven EUV sources.

Funding. Nederlandse Organisatie voor Wetenschappelijk Onderzoek (15697, 19458); European Research Council (802648).

Acknowledgments. This work was conducted at the Advanced Research Center for Nanolithography (ARCNL), a public private partnership between the University of Amsterdam (UvA), Vrije Universiteit Amsterdam (VU), Rijksuniversiteit Groningen (UG), the Dutch Research Council (NWO), and the semiconductor equipment manufacturer

Optics EXPRESS

ASML. This project has received funding from the European Research Council (ERC) Starting Grant number 802648 and is part of the VIDI research program with project number 15697, and the OTP grant with project number 19458, which are both financed by the Dutch Research Council (NWO). The authors thank Nik Noest and the AMOLF workshops for technical support.

Disclosures. The authors declare no conflicts of interest.

Data availability. Data underlying the results presented in this paper are not publicly available at this time but may be obtained from the authors upon reasonable request.

References

1. M. Ebrahim-Zadeh and I. T. Sorokina, *Mid-Infrared Coherent Sources and Applications* (Springer, 2008).
2. M. Ebrahim-Zadeh, A. S. Helmy, G. Leo, *et al.*, "Mid-infrared coherent sources and applications: introduction," J. Opt. Soc. Am. B **40**(1), MIC1 (2023).
3. F. K. Tittel, D. Richter, and A. Fried, *Mid-Infrared Laser Applications in Spectroscopy* (Springer Berlin Heidelberg, 2003), pp. 458–529.
4. S. Yang and Y. Shen, "Compact high-power MIR laser through pulse fiber laser pumped PPMgLN-based OPO," Appl. Opt. **64**(3), 603–608 (2025).
5. B. Wu, Y. Shen, and S. Cai, "Widely tunable high power OPO based on a periodically poled MgO doped lithium niobate crystal," Opt. Laser Technol. **39**(6), 1115–1119 (2007).
6. A. Zukauskas, N. Thilmann, V. Pasiskevicius, *et al.*, "5 mm thick periodically poled Rb-doped KTP for high energy optical parametric frequency conversion," Opt. Mater. Express **1**(2), 201–206 (2011).
7. Y. Liu, K. M. Mølster, A. Zukauskas, *et al.*, "Type-II PPRKTP optical parametric oscillators in the 2 µm spectral range," J. Opt. Soc. Am. B **40**(1), A36–A43 (2023).
8. M. Dunn and M. Ebrahimzadeh, "Parametric generation of tunable light from continuous-wave to femtosecond pulses," Science **286**(5444), 1513–1517 (1999).
9. D. Brida, C. Manzoni, G. Cirmi, *et al.*, "Few-optical-cycle pulses tunable from the visible to the mid-infrared by optical parametric amplifiers," J. Opt. **12**(1), 013001 (2010).
10. S. Chaitanya Kumar, A. Esteban-Martin, T. Ideguchi, *et al.*, "Few-cycle, broadband, mid-infrared optical parametric oscillator pumped by a 20-fs ti:sapphire laser," Laser Photonics Rev. **8**(5), L86–L91 (2014).
11. L. Behnke, R. Schupp, Z. Bouza, *et al.*, "Extreme ultraviolet light from a tin plasma driven by a 2-μm-wavelength laser," Opt. Express **29**(3), 4475–4487 (2021).
12. R. Schupp, F. Torretti, R. Meijer, *et al.*, "Efficient Generation of Extreme Ultraviolet Light From Nd:YAG-Driven Microdroplet-Tin Plasma," Phys. Rev. Appl. **12**(1), 014010 (2019).
13. L. Behnke, E. J. Salumbides, G. Göritz, *et al.*, "High-energy parametric oscillator and amplifier pulsed light source at 2-μm," Opt. Express **31**(15), 24142–24156 (2023).
14. R. A. Meijer, A. S. Stodolna, K. S. E. Eikema, *et al.*, "High-energy Nd:YAG laser system with arbitrary sub-nanosecond pulse shaping capability," Opt. Lett. **42**(14), 2758–2761 (2017).
15. Z. Mazzotta, J. Mathijssen, K. Eikema, *et al.*, "TI-REX: A tunable infrared laser for experiments in nanolithography," in *Conference on Lasers and Electro-Optics Europe and European Quantum Electronics Conference* (Optica Publishing Group, 2021), paper cd_p_28.
16. Z. Mazzotta, J. Mathijssen, O. Versolato, *et al.*, "TI-REX: a 5→20 ns temporally shapeable and 1.4–4.4µm wavelength-tunable source for nanolithography," in *High-brightness Sources and Light-driven Interactions Congress* (Optica Publishing Group, 2022), paper HW2B.2.
17. A. Zylstra, O. Hurricane, D. Callahan, *et al.*, "Burning plasma achieved in inertial fusion," Nature **601**(7894), 542–548 (2022).
18. H. Abu-Shawareb, R. Acree, P. Adams, *et al.*, "Achievement of target gain larger than unity in an inertial fusion experiment," Phys. Rev. Lett. **132**(6), 065102 (2024).
19. G. Arisholm, Ø. Nordseth, and G. Rustad, "Optical parametric master oscillator and power amplifier for efficient conversion of high-energy pulses with high beam quality," Opt. Express **12**(18), 4189–4197 (2004).
20. A. Godard, M. Guionie, J.-B. Dherbecourt, *et al.*, "Backward optical parametric oscillator threshold and linewidth studies," J. Opt. Soc. Am. B **39**(2), 408–420 (2022).
21. A. V. Smith, *Crystal Nonlinear Optics: with SNLO Examples* (AS-Photonics, 2018).
22. A. V. Smith, AS-Photonics, "SNLO nonlinear optics code," https://as-photonics.com/products/snlo/ (2023).
23. I. Tamer, B. A. Reagan, T. Galvin, *et al.*, "Demonstration of a compact multi-joule, diode-pumped Tm:YLF laser," Opt. Lett. **46**(20), 5096–5099 (2021).

193.87.134.36 2025-06-30 06:09:42